RESEARCH ARTICLE

A Study on Dual-Response Composite Hydrogels Based on Oriented Nanocellulose

Lina Dong[1,2†], Mujiao Liang[1,2†], Zhongwei Guo[1,2], Anyang Wang[2], Gangpei Cai[2], Tianying Yuan[1], Shengli Mi[2]*, Wei Sun[1,2,3,4]*

[1]Macromolecular Platforms for Translational Medicine and Bio-Manufacturing Laboratory, Tsinghua-Berkeley Shenzhen Institute, Shenzhen 518055, P.R. China
[2]Tsinghua Shenzhen International Graduate School, Tsinghua University, Shenzhen 518055, China
[3]Department of Mechanical Engineering, Biomanufacturing Center, Tsinghua University, Beijing, P.R. China
[4]Department of Mechanical Engineering, Drexel University, Philadelphia, PA, USA
[†]*These authors contributed equally to this work*

Abstract: In nature, many biological tissues are composed of oriented structures, which endow tissues with special properties and functions. Although traditional hydrogels can achieve a high level of biomimetic composition, the orderly arrangement of internal structures remains a challenge. Therefore, it is of great significance to synthesize hydrogels with oriented structures easily and quickly. In this study, we first proposed and demonstrated a fabrication process for producing a well-ordered and dual-responsive cellulose nanofibers + hyaluronic acid methacrylate (CN+HAMA) hydrogels through an extrusion-based three-dimensional (3D) printing process. CN in the CN+HAMA hydrogels are directionally aligned after extrusion due to shear stress. In addition, the synthesized hydrogels exhibited responsive behaviors to both temperature and ultraviolet light. Since the temperature-responsiveness is reversible, the hydrogels can transit between the gelation and solution states while retaining their original qualities. Furthermore, the developed well-oriented CN+HAMA hydrogels induced directional cell growth, paving the way for potential applications in ordered biological soft-tissue repair.

Keywords: Nanocellulose hydrogel; Directional arrangement; Thermal response; Ultraviolet response; 3D printing

*Correspondence to: Shengli Mi, Tsinghua Shenzhen International Graduate School, Tsinghua University, Shenzhen 518055, China; mi.shengli@sz.tsinghua.edu.cn; Wei Sun, Macromolecular Platforms for Translational Medicine and Bio-Manufacturing Laboratory, Tsinghua-Berkeley Shenzhen Institute, Shenzhen 518055, P.R. China: weisun@mail.tsinghua.edu.cn

Received: March 26, 2022; **Accepted:** April 21, 2022; **Published Online:** June 8, 2022

(This article belongs to the *Special Issue: Composite/Multi-component Biomaterial Inks and Bioinks*)

Citation: Dong L, Liang M, Guo Z, *et al.* A Study on Dual-Response Composite Hydrogels Based on Oriented Nanocellulose. *Int J Bioprint,* 8(3):578. http://doi.org/10.18063/ijb.v8i3.578

1. Introduction

Soft-tissue defects are often accompanied by deep tissue injuries, such as muscle, tendon, blood vessel, and nerve damage. This requires tissue repair and functional reconstruction and could lead to local inflammation if not handled properly[1]. Soft tissues in living organisms, such as muscles, nerve tissue, corneal tissue, tendons, and ligaments, have well-ordered microstructures with highly anisotropic properties. Defect repair and functional reconstruction of soft tissues with ordered structures is a problem that needs to be addressed. Therefore, it is crucial to find biocompatible materials for defect repair of soft tissues with ordered structures to achieve functional reconstruction[2].

Hydrogels, a kind of biomaterial with a three-dimensional (3D) crosslinking network structure composed of hydrophilic polymers, have been widely used to synthesize biomimetic structures in tissue engineering and regenerative medicine[3-5]. Cellulose is widely used in tissue engineering due to its good biocompatibility[6,7]. Cellulose nanofibers (CNs) are the most commonly used cellulose derivatives in the fabrication of composite hydrogels. Besides, CNs have been largely used for reinforcing filler to increase the mechanical properties of

hydrogels, due to their tensile strength and stiffness[8-10]. It has been reported that CNs can also increase the viscosity of hydrogels and enhance their printability, which is beneficial in extrusion printing[11]. CNs are one of the most promising fiber additives with multiple functions in 3D printing applications[12]. The polymer networks of CNs hydrogels are generally uniform and isotropic. Although traditional CNs hydrogels can achieve a high degree of biomimetic composition, they lack the ability to mimic the complex structure of biological tissues, for example, well-ordered structures[13]. Recently, several well-ordered hydrogels have been synthesized through directional freezing[14,15], electrostatic repulsion[16], magnetic methods[17], stain- or compression-induced reorientation[18], and self-assembly[19]. It has been reported in some literatures, epichlorohydrin was applied to form the loosely cross-linked points to mediate the cellulose chains' self-assembly and external stretching was used to promote fiber orientation[20-22]. Compared with the above cellulose hydrogels synthesis processes, epichlorohydrin and external force stretching were removed in our study. Inspired by the fact that external forces induce rearrangement of hydrogel structures, we used extrusion-based 3D printing process to promote fiber alignment[23]. Alignment of the CNs along the hydrogel flow direction occurs due to the shearing and extensional forces of the print nozzle[24]. Siqueira *et al*. reported a shape morphing and self-actuating alignment nanocellulose hydrogels prepared by extrusion-based 3D printing process[25]. On the other hand, hyaluronic acid (HA) is known to act as biocompatible and effectively adhesive material for various cells[26-28]. For instance, Xavier Acasigua *et al*. prepared natural bacterial cellulose/HA as scaffolds for culturing human dental pulp stem cells. The cells were adhered to the fibers and well distributed in composite scaffolds[29]. Fan *et al*. developed a mechanically reinforced hydrogel for the 3D culture of chondrogenic cells. In this model, CNs and GelMA/HAMA serve as the structural support while GelMA/HAMA as the cytogel containing a mouse chondrogenic cell line[30]. Zhao *et al*. developed nanocomposite hydrogels composed of methacrylate-functionalized CNs and HA methacrylate (HAMA), which provided a good microenvironment for bone marrow mesenchymal stem cell proliferation, as well as exhibited prominent repair effect in the cartilage defect[31].

In our study, the CNs showed a reversible state change with temperature. The reversible temperature-sensitive property of the CN-related hydrogel precursors enables them to gel *in situ* (at body temperature) and return to original liquid state at low temperatures. Besides, HAMA can respond quickly to ultraviolet (UV) irradiation. Therefore, temperature and UV dual-responsive CN+HAMA hydrogels are promising candidates for biomaterial inks in biofabrication[32,33]. Importantly, the CNs were aligned after extrusion. Furthermore, the printed well-oriented hydrogels induced L929 fibroblasts to grow in a specific direction, paving the way for potential use in ordered biological soft-tissue repair[34-36].

2. Materials and methods

2.1. Materials

(HA, MW 100-200 kDa) was purchased from Lifecore Biomedical (Chaska, MN, USA). Methacrylic anhydride and Irgacure 2959 were purchased from Sigma-Aldrich (St. Louis, MO, USA). The cotton linter pulps were provided by Hubei Chemical Fiber Group Ltd., (Xiangfan, China). Other analytical grade chemicals were purchased from Sinopharm Chemical Reagent Co., Ltd. (Shanghai, China).

2.2. Preparation of CN+HAMA hydrogel precursors and hydrogels

Lithium hydroxide (LiOH) (4.5 wt%) and urea (15 wt%) were dissolved in water and stirred sufficiently to obtain a homogenous solution. The cotton linter pulps were mechanically ground for 1 h. At freezing temperatures, cotton linter pulps were added to the mixed solution with vigorous stirring. After several freeze–thaw cycles and full stirring, a clear and transparent viscose solution of cellulose with a concentration of 4.5 wt% was obtained, and the concentration of CN (4.5 wt%) is kept constant across all formulations in the paper. The cellulose solution was ground using a super mass grinder to obtain CN suspension.

HAMA was synthesized according to a previously published procedure[37]. HAMA was added to the CN solution, and then, the system was stirred for 2–3 h under an ice bath to obtain different concentrations of the CN+HAMA solution. After full dissolution, the solution temperature was increased to 30°C to obtain CN+HAMA hydrogel precursors (**Figure S1**). CN+HAMA hydrogels were formed after irradiation with UV light (365 nm).

2.3. Characterization of hydrogels

Scanning electron microscopy (SEM, Zeiss/Sigma 300, America) was used to examine the morphology of the freeze-dried CNs, HAMA, and CN+HAMA hydrogels at different concentrations. All specimens were coated with a conductive layer of sputtered gold. An accelerating voltage of 5 kV and a working distance of 5 mm were applied.

2.4. Temperature and UV dual-responsiveness of CN+HAMA hydrogels

The prepared CN+HAMA hydrogel precursors of 1 mL were added into a straightly standing vial. To verify the reversible temperature-responsiveness of the hydrogel

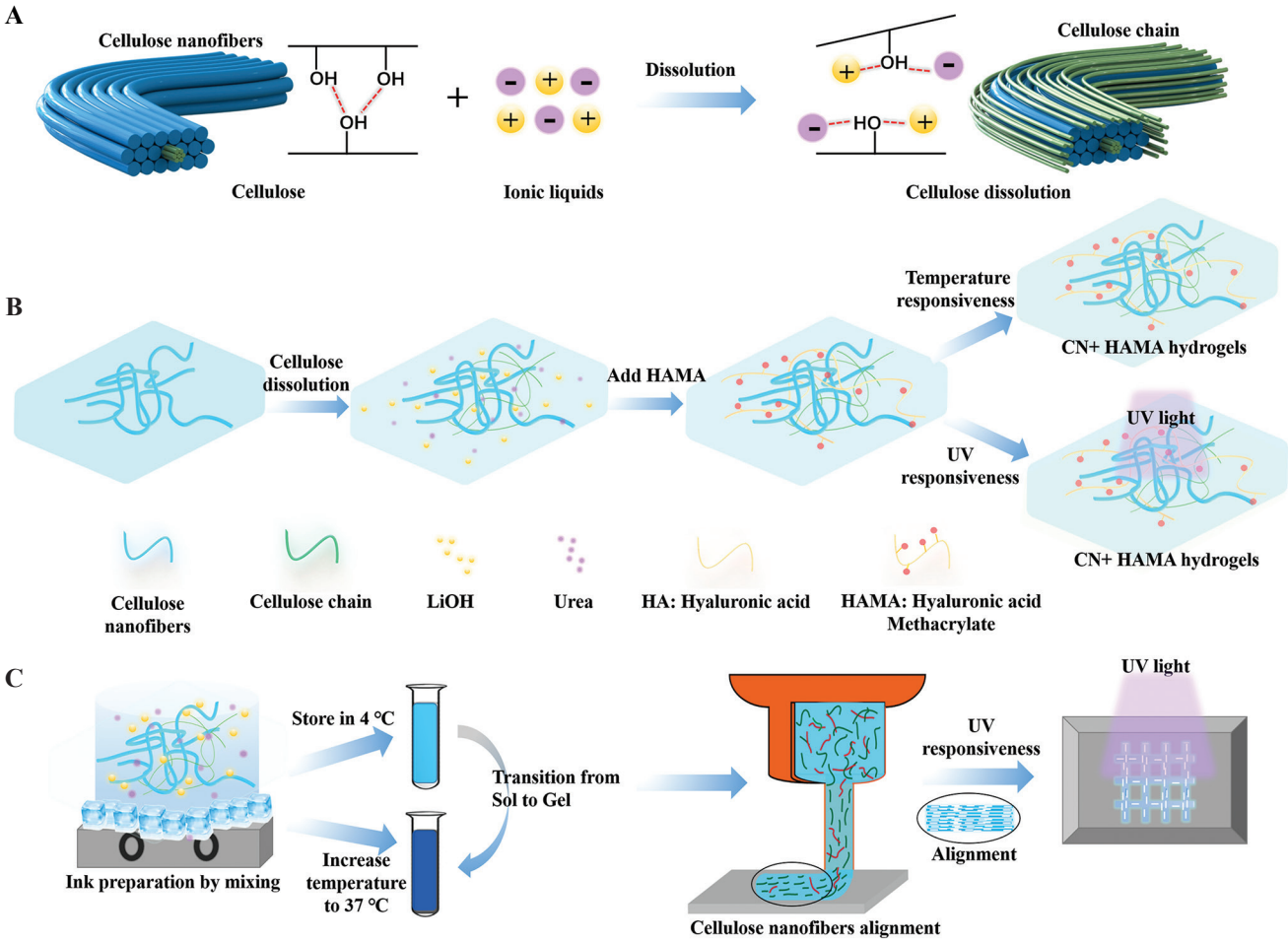

Figure 1. Schematic illustration of the composition and synthesis mechanism of the cellulose nanofibers + hyaluronic acid methacrylate (CN+HAMA) hydrogels. (A) Schematic diagram of the dissolution mechanism of cellulose. (B and C) Schematic diagram of the synthesis and curing process of the CN+HAMA hydrogels.

precursors, the precursors were not irradiated with UV light, and the state of the hydrogel precursors was changed by adjusting the temperature. The hydrogel precursors were placed in a cryogenic trap until the temperature reached 4°C, then the temperature was increased to 10°C. Next, the precursors were placed in a water bath at 25°C and 30°C. Followed, the precursors were then cooled to 0°C. The images of the vials were taken after they were placed on its side for 5 min.

To verify the UV secondary crosslinking performance of the hydrogels precursor, the temperature of the hydrogel precursors was maintained at 4°C, and hydrogel in the vial was irradiated with UV light for different durations. Then, the images of the vials were taken after they were placed on its side for 5 min.

2.5. Mechanical properties of CN+HAMA hydrogels

Compressive tests were performed using an Instron E3000 mechanical tester at a compression rate of 1 mm/min until the specimen fractured. The hydrogel specimens were cylindrical in shape (8 mm in diameter and 5 mm in height). The elastic modulus was calculated from the slope of the stress–strain curve in the 0 – 10% strain range. Three samples (n = 3) were used in the mechanical tests.

2.6. Rheological tests

A rheometer (MCR302, Anton Paae, Austria) equipped with a plate-plate geometry (25 mm in diameter, and 27 μm gap) was used to perform the rheological assays. The shear viscosity was measured at shear rates ranging from 1~100 s^{-1} at 25°C. A temperature sweep was performed at temperatures ranging from 0~40°C at 5% strain and 1% Hz. All of the tests were performed in the linear viscoelastic region. The tests were repeated 3 times for different hydrogels components.

2.7. Wide-angle X-ray diffraction (WAXD) test

To measure the degree of orientation of the CN+HAMA hydrogels before and after extrusion, two-dimensional

wide-angle X-ray diffraction (2D-WAXD) was performed. An in-house micro X-ray source (Incoatec, GmbH) with Cu Kα radiation (λ = 0.154 nm) was used. The scattering signal was collected by a multiwire proportional chamber detector (Bruker, Vantec-500) with a resolution of 2048*2048 pixels (pixel size of 68 μm). The distance between the sample and detector was fixed at 1038 mm.

2.8. 3D printing of the hydrogels

The hydrogel precursors were placed in a 5 mL syringe that was fixed to the extrusion printhead. Biomaker software was used to design the printing model, and a 3D printer (SunP CPD1/Biomaker) was used to print the designed hydrogel. A 25 G needle was used during the process. The materials were printed at different temperatures, with a printing speed of 5 mm/s, and an extrusion speed of 0.7 mm^3/s. The hydrogel underwent shear thinning inside the extrusion needle and regained its viscosity outside the extrusion needle. Therefore, the hydrogel could be printed as one-dimensional (1D) filaments or 3D structures. After printing, the printed structures were exposed to UV light to enhance their stability.

2.9. Cell seeding and cell cultures on scaffolds

Mouse fibroblasts (L929 cells) were cultured in Roswell Park Memorial Institute (RPMI 1640) medium with 10% fetal bovine serum at 37°C and 5% CO_2. Before cell seeding, the CN+HAMA hydrogels scaffolds were immersed in 75% ethanol overnight and then exposed to UV light for 1 h. After UV irradiation, the scaffolds were washed 3 times with phosphate-buffered saline (PBS). An L929 cell suspension with a density of 3×10^6 cells/mL was seeded onto the scaffold. The scaffolds were cultured at 37°C with 5% CO_2, and the medium was changed 3 times per week.

2.10. Live/dead staining and cytoskeletal staining of cell-seeded scaffolds

The culture medium was removed from the L929 cell-seeded scaffolds, and then, the scaffolds were washed with 1 × PBS 3 times (5 min each time). Calcein-AM/ethidium homodimer dye was added for 15 min to stain the live/dead cells on the scaffolds. Phalloidin and DAPI dye were added for 1 h to stain the cytoskeleton of the cells on the scaffolds. The results were observed with a fluorescence microscope (Leica, DMi8).

2.11. Cytotoxicity test

L929 cells with a cell density of 4×10^4/mL were seeded into a 48-well plate and incubated for 24 h. Various concentrations of the cross-linked CN+HAMA hydrogels scaffold sheets with a diameter of 8 mm and a thickness of 2 mm were added to the cell medium in different wells. After coculture for 1, 3, and 7 days, cell counting kit-8 (CCK-8) solution was added to each well and incubated for 2 h. Subsequently, the reaction solution transferred to another 96-well plate, the optical density (OD) of the solution was measured by a spectrophotometer at 450 nm[38].

2.12. Animal experiment *in vivo*

All procedures were performed with the approval of the Animal Ethics Committee of Tsinghua Shenzhen International Graduate School, Tsinghua University. *In vivo* biosafety experiments were tested through subcutaneous implantation of Kunming mice (KM). The CN+HAMA hydrogels were cut into slices 10 mm in diameter and 1 mm in height. A small incision was made in the back of each mouse to insert a slice of the hydrogel. The wound was stitched up after the hydrogel was inserted. After 1 week, 3 weeks, and 10 weeks of implantation, skin and mucous tissue on the wound side, including the inserted hydrogel slices or not, were removed to perform hematoxylin-eosin (H&E) staining and immunofluorescence staining. H&E staining was performed according to the manufacturer's instructions. Immunofluorescence staining was performed with CD3 (goat anti-rabbit, Servicebio, and GB13014) and CD68 (goat anti-rabbit, Servicebio, and GB113109) as primary antibodies, anti-goat as secondary antibodies, and DAPI (Servicebio, G1012). A fluorescence microscope (Leica, DMi8) was used to image the immunofluorescence of the tissue sections.

2.13. Statistical analysis

All data were expressed as at least three independent experiments. Except that data analyzed in **Figure 2o** was using one-way analysis of variance (ANOVA), all the data elsewhere were analyzed using two-way ANOVA. Significant differences were indicated at $*P < 0.05$ and $**P < 0.01$.

3. Results and discussion

3.1. The design of the CN+HAMA hydrogels

As previously reported, the solvent alkali and urea can dissolve nanocellulose at low temperatures[39]. Active alkali hydrates were combined with cellulose and added to the solvent. Urea hydrates served as hydrogen-bonding donors and receptors, preventing cellulose molecules from coming into contact with one another. The nanocellulose molecular chain was untangled, and the solvent had a good dispersion of nanocellulose (**Figure 1a**). While dissolving cellulose, a thermosensitive phenomenon occurred, and the nanocellulose solution was in the liquid stage at low temperatures (≈ 4°C). When the temperature increased to body temperature (>30°C), the cellulose solution

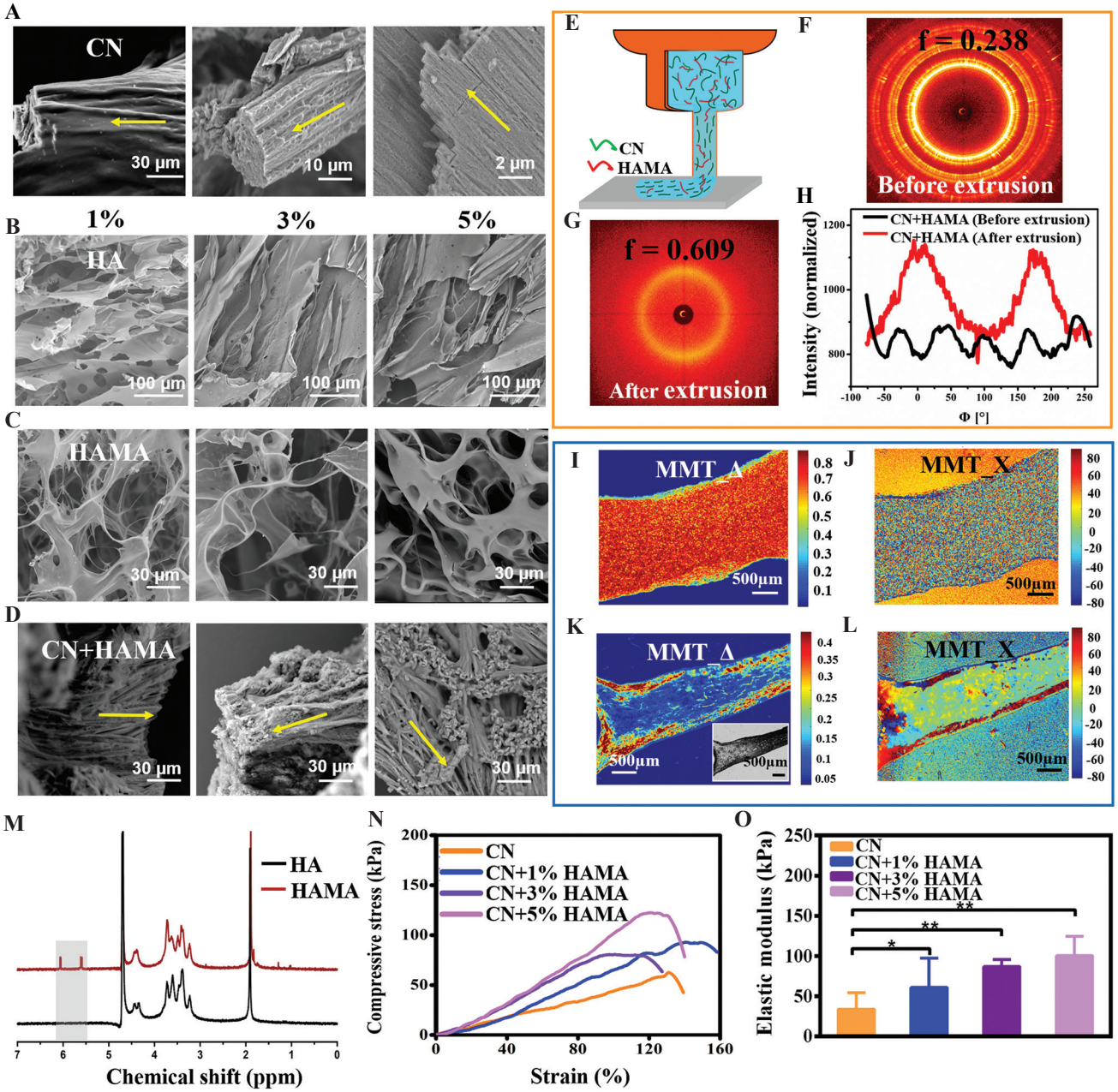

Figure 2. Cellulose nanofibers (CN) orientation within 3D-printed CN + hyaluronic acid methacrylate (CN+HAMA) hydrogels. SEM images of (A) CNs, (B) hyaluronic acid (HA), (C) HAMA, and (D) CN+HAMA hydrogels with different concentration ratios (The direction of yellow arrows represent the alignment of the fibers). (E) Schematic diagram of the direct writing process of CN+HAMA hydrogels. 2D-WAXS patterns of CN+HAMA hydrogels before extrusion (F) and after extrusion (G) from the nozzle. (H) Normalized 2D-WAXS azimuthal intensity distributions of the equatorial refection of CN+HAMA hydrogels before and after extrusion from the nozzle. Mueller matrix microscopy images of CN+HAMA hydrogels (I and J) before and (K and L) after extrusion under cross-polarized light. (M) ^{1}H NMR spectrum of HA, HAMA. (N) The compressive stress–strain curves and (O) elastic moduli of various hydrogels. (*$P < 0.05$, **$P < 0.01$).

gelled due to self-association interactions between cellulose aggregation. Consequently, CN hydrogel precursors performed temperature responsive property and can be cross-linked by thermal gelation, which helps to maintain structures during printing. However, the printed structures with temperature-induced gelation were unstable. To address this issue, HA was modified with photopolymerizable methacryloyl groups to allow UV secondary photo cross-linking during printing. Two types of cross-linking processes were used to increase the stability of the structure. Mouser *et al*. added HAMA to pHPMA-lac-PEG hydrogels to enhance printability and allow bioprinting with sufficient shape- stability of hydrogels[40].

As shown in **Figure 1b**, CN+HAMA hydrogels consisting of CNs and HAMA were designed to achieve temperature/UV dual-responsiveness. The dual-responsiveness of the CN+HAMA hydrogels could induce gelation *in situ* (body temperature). These properties pave the way for potential applications in soft-tissue repair. In **Figure 1c**, the CN+HAMA mixture was in a liquid state at a low temperature of 4°C and solidified as the temperature increased to 37°C. When the nanocellulose inside the hydrogel was extruded through a 3D printing nozzle, the internal structure was rearranged from a random order to directional alignment. To optimize the degree of nanocellulose alignment, the shear stress of the nozzle (τ_{max}) during extrusion was calculated with the equation[41]. $\tau = \Delta P \cdot r/2L$, where ΔP is the maximum pressure, applied at the nozzle ($\Delta P = 1.132 \times 10^6$ Pa). r is the radius of the nozzle ($r = 1.25 \times 10^{-4}$ m), and L is the nozzle length ($L = 1.277 \times 10^{-2}$ m). After the above formula calculation, we got the $T_{max} = 6460$ Pa. As shown in **Figure S2**, the maximum pressure applied at the nozzle exceeded the yield stress of each of the three concentrations (0%, 1%, and 3%) of CN+HAMA hydrogels, resulting in differential flow ($\tau < \tau_{max}$). The nanocellulose in these three hydrogel concentrations could be oriented after extrusion in 3D printing. The hydrogels were exposed to secondary UV curing after extrusion from nozzle.

3.2. Printed-induced quantified CN+HAMA alignment and characterization

To confirm our hypothesis, we first improved the synthesis method of cellulose hydrogel and synthesized HAMA according to previously published reports[37]. Furthermore, we synthesized temperature-sensitive CNs by utilizing the temperature change during the synthesis process. SEM images show that the synthesized cellulose fibers were neatly oriented after extrusion and that HAMA had a honeycomb porous structure (**Figure 2a-d**). The inner structure of CN+HAMA composite hydrogels after extrusion had neat and directional alignment. Furthermore, as shown in **Figure S3**, the prepared CN+1%HAMA hydrogel structure had a grooved and ridged nanosurface, the inner structures are nanofibers directional alignment.

To explore the flow-induced orientation of CN+HAMA hydrogels, we carried out two-dimensional (2D)-WAXD measurements and Mueller matrix imaging of the CN+HAMA hydrogels before and after extrusion. The CNs disordered inside the container and gradually aligned during the extrusion process (**Figure 2e**). As shown in **Figure 2h**, the degree of orientation (π) was calculated based on the azimuthal integration. In addition, the Herman's order parameter (f) value reflects the orientation degree: the larger the f value is, the greater the orientation of the nanocellulose alignment. According to the calculations shown in the Supplementary File, the CN+HAMA hydrogels were neater and more directionally aligned after extrusion (π = 68%, f = 0.28) (**Figure 2g**) from the nozzle than before extrusion (f = 0.06, **Figure 2f**), which was consistent with the previous results[25]. The results proved that CNs in the hydrogels can be aligned after extrusion from the nozzle.

To further evaluate the orientation effects of the CN+HAMA hydrogels, we used a Mueller matrix imaging microscope to analyze the inner fiber arrangement. The depolarization of the whole sample area was high before hydrogel extrusion (**Figure 2i**). In addition, the birefringent samples had different directions and arrangements, and the internal structure was homogeneously arranged (**Figure 2j**). After hydrogel extrusion, the depolarization of the sample center area was reduced (**Figure 2k**) and the angle of the hydrogel aligned along the axial direction was reduced, with a fiber alignment angle of approximately 20° (**Figure 2l**). The Mueller matrix data show that the fibers were arranged in the same direction after extrusion, indicating that the alignment of the CNs in the hydrogel was more regular than that before extrusion. In addition, the ^{1}H NMR spectrum of HAMA shows the existence of peaks at 5.4 and 5.6 ppm, which corresponded to the double bonds of methacrylamides (**Figure 2m**). In addition, the mechanical properties of the synthesized hydrogels were determined through the compressive stress−strain curves and elastic moduli. As demonstrated from the results (**Figure 2n and o**), the mechanical properties of the CN+1%HAMA hydrogels were 50% higher than those of the CN hydrogels. As the concentration of HAMA increased, the elastic moduli of the CN+HAMA hydrogels increased.

3.3. Temperature and UV dual-responsiveness of CN+HAMA hydrogels

In addition to the directional arrangement mode, the CN+HAMA hydrogels demonstrated reversible temperature sensitivity. The CN+HAMA hydrogels were treated with different temperatures and UV conditions, and the hydrogels showed different gel states, which indirectly proved their dual-responsiveness (UV response and thermal response). **Figure 3a** shows that the CN-related hydrogel precursors underwent reversible solution-gelation conversion with as the temperature changed. When the temperature was low, the hydrogel precursors were in a solution state similar to a liquid; when the temperature was high, at approximately 30°C, they formed solid gels. Next, we tested the UV (intensity=15 mW/cm^2) response performance of the hydrogels at 4°C (**Figure 3b**). The CN-related hydrogels maintained their state regardless of how long they were exposed to UV light. In contrast, the HAMA-related hydrogels solidified under UV irradiation for various times, after which the hydrogels remained in a solid gel state. **Figure 3b** indicates that the curing time

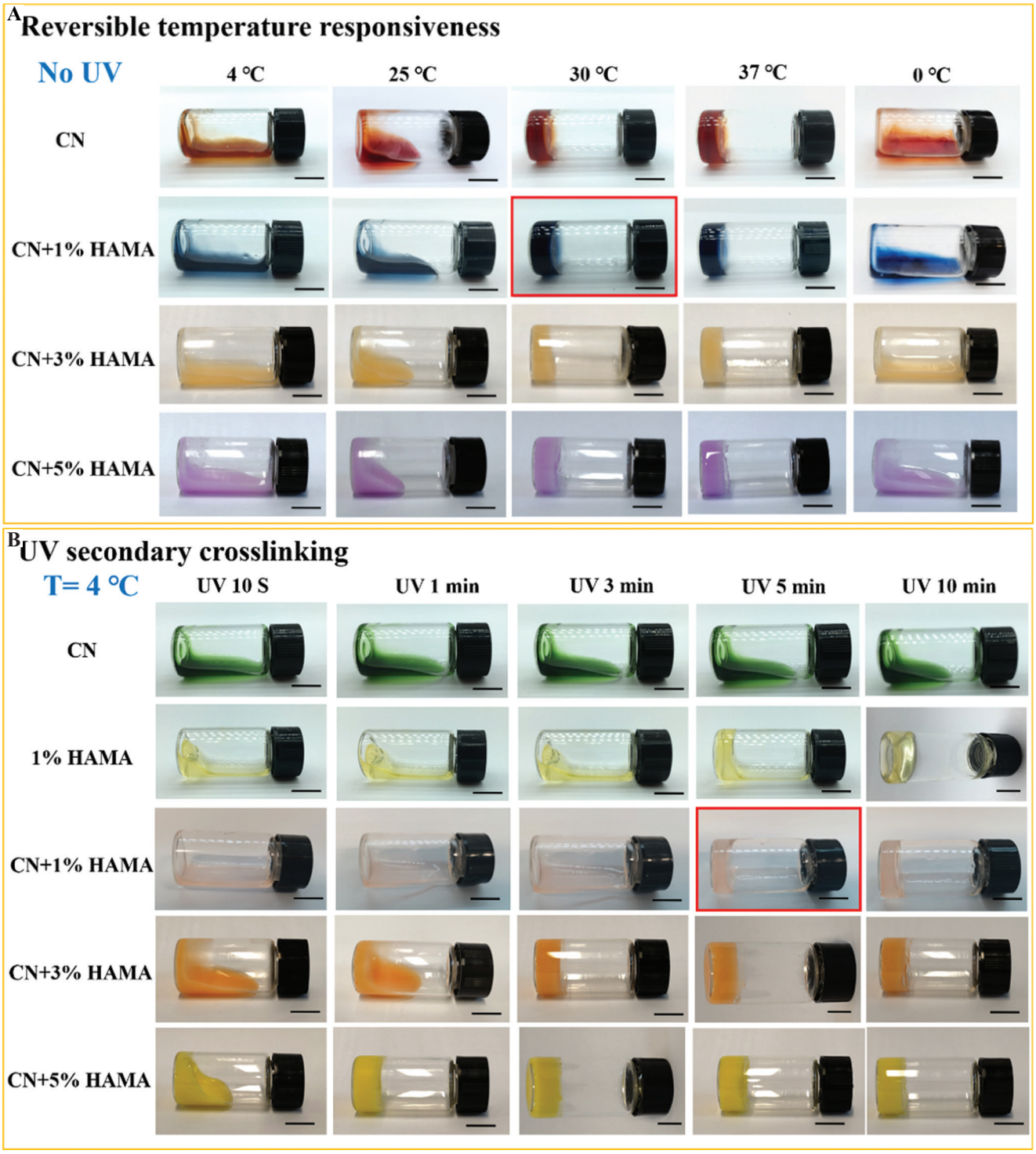

Figure 3. Images of various hydrogels under different conditions in vials on their sides. Scale bar is 1 cm. (A) The state of the hydrogel changed with temperature before UV irradiation. (B) The state of the hydrogel changed with UV irradiation time when the temperature was 4°C.

decreased as the concentration of HAMA increased, and for CN+1%HAMA hydrogels, the curing time was 5 min. As a control, CN-related hydrogels were reversibly temperature-sensitive, whereas MA-related hydrogels solidified after UV irradiation. After 5 min of UV irradiation, the cured hydrogel remained solid at various ambient temperatures (**Figure S4**). Therefore, the optimal parameters for CN+1%HAMA hydrogels in the next 3D printing step were 30°C and 15 mW/cm^2 UV irradiation for 5 min. The responsiveness of CN+1%HAMA to temperature and UV irradiation allows it to be used as a type of controllable printed biomaterial inks.

3.4. Shear-thinning, thermosensitivity, and printability of CN+HAMA hydrogel precursors

The CN+HAMA hydrogel precursors before UV cross-linking exhibited different properties under different temperature treatments. Through rheological measurements and differential scanning calorimetry, CN+HAMA hydrogel precursors demonstrated shear-thinning and thermal response properties, which corresponded with the results shown in **Figure 3**. As further demonstrated in **Figure 4a**, the shear-thinning behavior of hydrogel precursors at high shear rates, with the curves indicating that the precursors could be used for printing at equivalent shear rates. In addition, **Figure 4b** shows the oscillatory temperature sweeps of the four different hydrogel precursors. For all samples, the G' and G″ of the CN+HAMA hydrogels precursors increased with the temperature, which can be ascribed to the temperature-dependent property of the CN hydrogel precursors[42,43]. The CN and CN+1%HAMA hydrogel precursors were in liquid states below 30°C. The data suggested that CN and CN+1%HAMA hydrogel precursors gelled due to self-association interactions between cellulose aggregates above 37°C. Furthermore, at elevated temperatures, the combination of LiOH and urea hydrate on the cellulose chain was disturbed. Due to the self-binding force of cellulose, cellulose molecules connected, forming a network structure. In addition, the CN+3%HAMA and CN+5%HAMA hydrogel precursors were both in the gelation state due to their high concentrations. Collectively, CN+1%HAMA hydrogel precursors are appealing, because they can transit from a liquid state at low temperatures to a gel state at elevated temperatures (**Figure 4c**). Compared with the other hydrogels, the temperature change results revealed that the CN+1%HAMA precursors were clearly thermally responsive.

Due to their thermal responsiveness, CN+HAMA hydrogel precursors could adjust and physically cross-linked during 3D printing by thermal gelation, which helped to maintain the shapes of the printed structures. According to the rheological curves and thermal analysis results, the thermosensitive CN+1%HAMA precursors exhibited the optimal printability at approximately 30°C. To prove this, we printed hydrogels at various concentrations and different temperatures. From **Figure 4d**, it was clear that the printed grid structure of CN+1%HAMA precursors had the most uniform lines and most stable structure at 30°C. The printed structure of the other groups exhibited unclear lines and forms, because the concentration was so high that the ink coalesced and was extruded unequally. The results again proved that CN+1%HAMA precursors were the most appropriate ink for 3D printing.

3.5. Orientation structure alignment induces directional cell alignment

Ideal biomaterial inks should possess acceptable cytocompatibility. To investigate the cell safety of CN+HAMA hydrogels, we assessed the cytotoxicity with L929 cells. Based on the above evaluation of the printing effect, grid scaffolds printed with CN+1%HAMA hydrogels were used to further investigate the biocompatibility of printed hydrogels. Therefore, we began testing the cell safety of the hydrogels after obtaining the printed scaffolds. The CN+1%HAMA hydrogel-printed scaffold stabilized with UV irradiation and then seeded with L929 cells. Specifically, to measure the viability of the cells, scaffolds were fluorescence imaged after 1, 3, and 7 days in culture by staining cells with calcein-AM (green) and ethidium homodimer (red) (**Figures 5b-d and S5**). The results demonstrated that the 3D-printed scaffolds supported cell adhesion by allowing cells to extend projections. The cells adhered to the scaffold and multiplied with increasing culture time.

The cytotoxicity results revealed that the difference between the CN+1%HAMA hydrogels and the no pattern group was not significant, and compared with the other types of hydrogels, the CN+1%HAMA hydrogels had the highest cell viability (**Figure 5e**). To check the cytoskeleton of the cells, scaffolds were also imaged after 3 days (**Figure S6**) in culture by staining cells with phalloidin (green) and DAPI (blue). As expected, the morphology of L929 cells did not change significantly in the culture with 3D-printed scaffolds. These data suggested that the printed CN+1%HAMA hydrogel scaffold had low *in vitro* cytotoxicity and no effect on cell proliferation.

As shown in **Figure S3**, the prepared CN+1%HAMA hydrogel scaffold had ridge and groove nanosurface. When cells recognize the surface characteristics of the hydrogel, they can respond to the micro-nano-scale surface of the topological structure and produce a contact guidance effect[44]. The grooves of the material surface can affect the arrangement balance between cells and force cells to rearrange to adapt to the contacted material. Cells can adjust their size and orientation along the groove direction. The microstrips on the surface of the hydrogel can regulate the signal transduction of cells and matrix, affecting the cell's adhesion, the development of cytoskeleton and the movement of the cell, thereby forming highly-oriented cells patterns[45,46]. As shown in **Figure 5g**, the L929 cells were seeded on the CN+1%HAMA hydrogel scaffold for 7 days and rearranged to adapt to the contacted hydrogel. Cells could adjust their size and orientation along the groove direction, eventually forming a cell arrangement layer parallel to the CN direction in the hydrogel (**Figure 5a**). The L929 cells grew and arranged in one direction, forming oriented

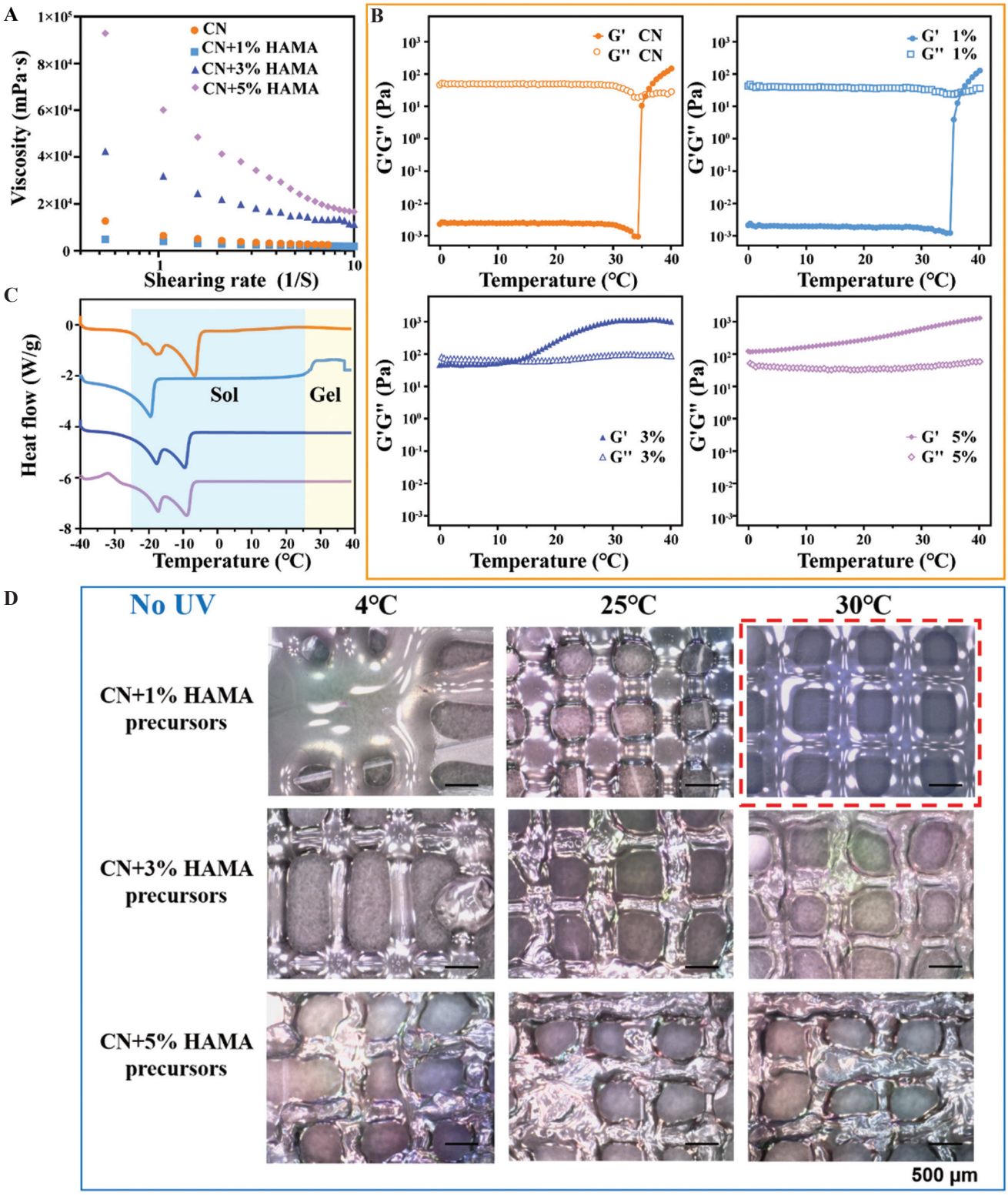

Figure 4. Rheological evaluation and differential scanning calorimetry (DSC) of CN+HAMA hydrogel precursors before UV cross-linking. (A) Continuous flow tests of various hydrogel precursors at shear rates of 0-10 s^{-1}. (B) Temperature sweep of various hydrogel precursors (G': storage modulus, G'': loss modulus). (C) DSC curves of various hydrogels precursors. (D) Images of 3D-printed grid structures of various CN+HAMA hydrogel precursors before UV cross-linking in different temperature environments.

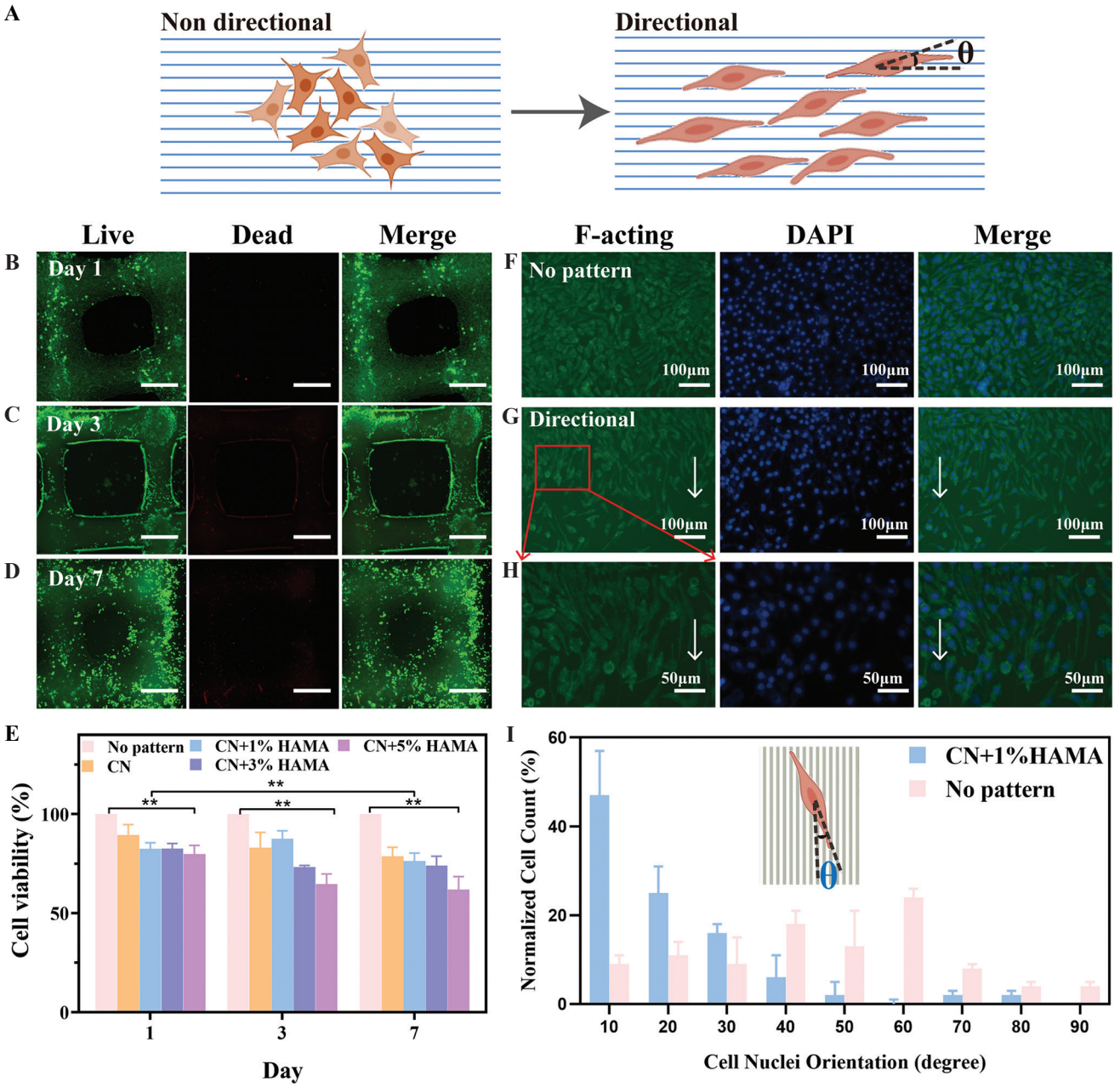

Figure 5. CN+1%HAMA hydrogels induce directional growth of L929 cells. (A) Schematic diagram of the growth process of cells on the surface of oriented fibers. (B) Day 1, (C) Day 3, and (D) Day 7 fluorescence images of printed scaffolds seeded with L929 cells with live/dead stain. The scale bar is 500 μm. (E) Cell viability comparison between various hydrogels on different days (Days 1, 3, and 7), measured by a CCK-8 assay. (*$P < 0.05$, **$P < 0.01$). (F) The growth process of L929 cells seeded on culture dishes without treatment. (G) The growth process of cells seeded on printed CN+1%HAMA hydrogel scaffolds. (H) A zoomed-in view of the frame column section in **Figure 6g**. (I) Orientation angle distribution of L929 cells on CN+1%HAMA hydrogel scaffolds after culturing for 7 days.

cell patterns when cultured on CN+1%HAMA hydrogels (**Figure 5g and h**). **Figure 5f** shows that the L929 cells grew in all directions when they were cultured on petri dishes without any treatment. These results verified that the unique orientation structure of the CN+1%HAMA hydrogels affected cell adhesion and promoted the arranged orientation of L929 cells, suggesting potential functions for improving cell alignment *in vitro*. This work provides new structure-oriented hydrogel applications in tissue engineering.

3.6. *In vivo* safety

An *in vitro* cell assay and an *in vivo* animal experiment were carried out to illustrate the biocompatibility and

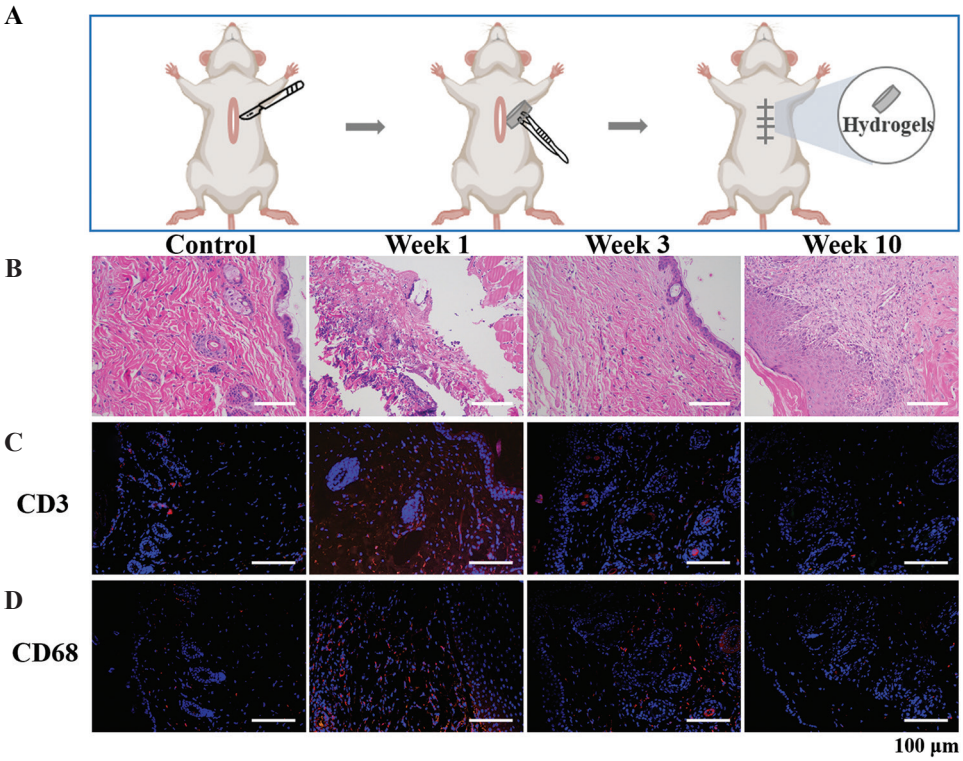

Figure 6. Biosafety and characterization of CN+1%HAMA hydrogels in Kunming Mouse models. (A) Schematic illustration of implanting hydrogel samples in Kunming mouse models. Subcutaneously implanted hydrogels were explanted with the surrounding tissue after 1, 3, or 10 weeks. Sections were subjected to H&E staining (B) and stained red for CD3 (C) or CD68 (D) antigens.

safety of CN+1%HAMA hydrogels. The *in vivo* biosafety of CN+1%HAMA hydrogels was tested by implanting hydrogel samples in Kunming mouse models and monitoring the inflammatory response over 10 weeks. We subcutaneously implanted sterile hydrogel samples or blank controls in the back skin of mice (**Figure 6a**). We ensured that the mice remained healthy throughout the experiment until they were sacrificed for euthanasia.

To evaluate the toxic side effects of the CN+1%HAMA hydrogels, we, further, performed the H&E staining and immunofluorescence staining of the tissue around the implantation site. **Figure 6b** clearly shows that many inflammatory cells, including lymphocytes and macrophages, had infiltrated the tissue 1 week after implantation. Only a few inflammatory cells were found at 3 weeks. No toxicity or inflammatory cells were observed in the implantation site at 10 weeks (n = 5). In addition, **Figure 6c** and **6d** show the results of immunofluorescence staining of T-cells with CD3 antigen and macrophages with CD68 antigen, both of which were colored red. The results were consistent with those of H&E staining. T-cells and macrophages were observed after 1 week. This is because the immune systems of the mice responded to foreign implants after 1 week. Compared to 1 week, the T-cell and macrophage signals were greatly reduced after 3 weeks, which demonstrated that the immunoreaction was greatly reduced after 3 weeks. The images show little signal of both kinds of cells, which indicated that the inflammatory response was gone and that CN+1%HAMA hydrogels do not cause tissue damage *in vivo*. Therefore, it is reasonable to assume that the biodegradability and biosafety of CN+1%HAMA hydrogels could allow them to be used in tissue engineering and regenerative medicine.

4. Conclusions

In this study, we successfully developed a novel CN+HAMA hydrogels with thermo- and UV light-responsive capabilities. The nanocellulose was thermosensitive, with a fluid state at low temperatures and a gel state at body temperature (>30°C). This reversible change allows the hydrogels to gel *in situ* at temperatures >30°C while maintaining stability at low temperatures (even below 0°C). In addition, the incorporation of a UV-cross-linked HAMA polymer network could improve the temperature-responsiveness of the system. Furthermore, the CNs could be aligned directionally due to the shear stress-induced by the extrusion process. As a result, the cells seeded on the printed scaffold grew directionally, which indicated that the hydrogels could be used as potential candidate ink for the fabrication of oriented soft-tissue mimics.

The injectable, oriented, and dual-responsive hydrogels were composed of natural and bioextractive materials and exhibited good biocompatibility, which is essential for biofabrication. In summary, our work provides a new printable ink with characteristics such as structure orientation, dual-responsiveness (temperature and UV), and biocompatibility, which will promote the exploration of highly-oriented biological tissue repair.

Acknowledgment

The authors acknowledge financial support from the Tsinghua Berkeley Shenzhen Institute and the Project of Basic Research of Shenzhen, China (JCYJ20170412101508433 and JCYJ20180507183655307).

Funding

The research reported in this publication was supported by funding from the Tsinghua Berkeley Shenzhen Institute and the Project of Basic Research of Shenzhen, China (JCYJ20170412101508433 and JCYJ20180507183655307).

Conflict of interest

The authors declare no competing financial interest.

References

1. Powers DB, Breeze J, 2019, Avulsive Soft Tissue Injuries. *Atlas Oral Maxillofac Surg Clin*, 27:135–42. https://doi.org/10.1016/j.cxom.2019.05.005
2. Brown BN, Badylak SF, 2014, Extracellular Matrix as an Inductive Scaffold for Functional Tissue Reconstruction. *Transl Res*, 163:268–85. https://doi.org/10.1016/j.trsl.2013.11.003
3. Lee KY, Mooney DJ, 2001, Hydrogels for Tissue Engineering. *Chem Rev*, 101:1869–79.
4. Zhang YS, Khademhosseini A, 2017, Advances in Engineering Hydrogels. *Science*, 356:eaaf3627.
5. Hoffman AS, 2012, Hydrogels for Biomedical Applications. *Adv Drug Deliver Rev*, 64:18–23.
6. Tavakolian M, Jafari SM, van de Ven TG, 2020, A Review on Surface-Functionalized Cellulosic Nanostructures as Biocompatible Antibacterial Materials. *Nano-Micro Lett*, 12:73. https://doi.org/10.1007/s40820-020-0408-4
7. Hai Van H, Makkar P, Padalhin AR, *et al.*, 2020, Preliminary Studies on the *in Vivo* Performance of Various Kinds of Nanocellulose for Biomedical Applications. *J Biomater Appl*, 34:942–51. https://doi.org/10.1177/0885328219883478
8. De France KJ, Hoare Tand Cranston E D, 2017, Review of Hydrogels and Aerogels Containing Nanocellulose. *Chem Mater*, 29:4609–31. https://doi.org/10.1021/acs.chemmater.7b00531
9. Ravanbakhsh H, Bao G, Luo Z, *et al.*, 2021, Composite Inks for Extrusion Printing of Biological and Biomedical Constructs. *ACS Biomater Sci Eng*, 7:4009–26. https://doi.org/10.1021/acsbiomaterials.0c01158
10. Tashiro K, Kobayashi M, 1991, Theoretical Evaluation of 3-Dimensional Elastic-constants of Native and Regenerated Celluloses-role of Hydrogen-bonds. *Polymer*, 32:1516–30. https://doi.org/10.1016/0032-3861(91)90435-l
11. Mueller M, Ozturk E, Arlov O, *et al.*, 2017, Alginate Sulfate-Nanocellulose Bioinks for Cartilage Bioprinting Applications. *Ann Biomed Eng*, 45:210–23. https://doi.org/10.1007/s10439-016-1704-5
12. Chinga-Carrasco G, 2018, Potential and Limitations of Nanocelluloses as Components in Biocomposite Inks for Three-Dimensional Bioprinting and for Biomedical Devices. *Biomacromolecules*, 19:701–11. https://doi.org/10.1021/acs.biomac.8b00053
13. Yadav S, Majumder A, 2021, Biomimicked Hierarchical 2D and 3D Structures from Natural Templates: Applications in Cell Biology. *Biomed Mater*, 16:7. https://doi.org/10.1088/1748-605x/ac21a7
14. Hua M, Wu S, Ma Y, *et al.*, 2021, Strong Tough Hydrogels Via the Synergy of Freeze-casting and Salting Out. *Nature*, 590:594–9. https://doi.org/10.1038/s41586-021-03212-z
15. Zhang H, Cooper AI, 2007, Aligned Porous Structures by Directional Freezing. *Adv Mater*, 19:1529–33. https://doi.org/10.1002/adma.200700154
16. Liu M, Ishida Y, Ebina Y, *et al.*, 2015, An Anisotropic Hydrogel with Electrostatic Repulsion between Cofacially Aligned Nanosheets. *Nature*, 517:68–72. https://doi.org/10.1038/nature14060
17. Kuo JC, Huang HW, Tung SW, *et al.*, 2014, A Hydrogel-based Intravascular Microgripper Manipulated using Magnetic Fields. *Sensor Actuat Phys*, 211:121–30. https://doi.org/10.1016/j.sna.2014.02.028
18. Shikinaka K, Koizumi Y, Kaneda K, *et al.*, 2013, Strain-induced Reversible Isotropic-anisotropic Structural Transition of Imogolite Hydrogels. *Polymer*, 54:2489–92. https://doi.org/10.1016/j.polymer.2013.03.028
19. Shao JJ, Raidongia K, Koltonow AR, *et al.*, 2015, Self-assembled Two-dimensional Nanofluidic Proton Channels with High Thermal Stability. *Nat Commun*, 6:7602–2.

https://doi.org/10.1038/ncomms8602

20. Guo J, Li Q, Zhang R, *et al.*, 2022, Loose Pre-cross-linking Mediating Cellulose Self-assembly for 3D Printing Strong and Tough Biomimetic Scaffolds. *Biomacromolecules*, 23:877-88. https://doi.org/10.1021/acs.biomac.1c01330.s002
21. Ye D, Yang P, Lei X, *et al.*, 2018, Robust Anisotropic Cellulose Hydrogels Fabricated via Strong Self-aggregation Forces for Cardiomyocytes Unidirectional Growth. *Chem Mater*, 30:5175–83. https://doi.org/10.1021/acs.chemmater.8b01799
22. Zou J, Wu S, Chen J, *et al.*, 2019, Highly Efficient and Environmentally Friendly Fabrication of Robust, Programmable, and Biocompatible Anisotropic, All-Cellulose, Wrinkle-Patterned Hydrogels for Cell Alignment. *Adv Mater*, 31:1904762. https://doi.org/10.1002/adma.201904762
23. Kong W, Wang C, Jia C, *et al.*, 2021, Muscle-inspired Highly Anisotropic, Strong, Ion-Conductive Hydrogels. *Adv Mater*, 33:1801934–41. https://doi.org/10.1002/adma.201801934
24. Ma T, Lv L, Ouyang C, *et al.*, 2021, Rheological Behavior and Particle Alignment of Cellulose Nanocrystal and its Composite Hydrogels During 3D Printing. *Carbohyd Polym*, 253:117217. https://doi.org/10.1016/j.carbpol.2020.117217
25. Fourmann O, Hausmann MK, Neels A, *et al*., 2021, 3D Printing of Shape-morphing and Antibacterial Anisotropic Nanocellulose Hydrogels. *Carbohydr Polym*, 259:117716–27. https://doi.org/10.1016/j.carbpol.2021.117716
26. Collins MN, Birkinshaw C, 2013, Hyaluronic Acid Based scaffolds for Tissue Engineering a Review. *Carbohyd Polym*, 92:1262–79. https://doi.org/10.1016/j.carbpol.2012.10.028
27. Gwak MA, Hong BM, Seok JM, et al., 2021, Effect of Tannic Acid on the Mechanical and Adhesive Properties of Catechol-modified Hyaluronic Acid Hydrogels. *Int J Biol Macromol*, 191:699–705. https://doi.org/10.1016/j.ijbiomac.2021.09.123
28. Shin J, Lee JS, Lee C, et al., 2015, Tissue Adhesive Catechol-Modified Hyaluronic Acid Hydrogel for Effective, Minimally Invasive Cell Therapy. *Adv Funct Mater*, 25:3814–24. https://doi.org/10.1002/adfm.201500006
29. Xavier Acasigua GA, de Olyveira GM, Manzine Costa LM, *et al.*, 2014, Novel Chemically Modified Bacterial Cellulose Nanocomposite as Potential Biomaterial for Stem Cell Therapy Applications. *Curr Stem Cell Res T*, 9:117–23. https://doi.org/10.2174/1574888x08666131124135654
30. Fan Y, Yue Z, Lucarelli E, *et al.*, 2020, Hybrid Printing Using Cellulose Nanocrystals Reinforced GelMA/HAMA Hydrogels for Improved Structural Integration. *Adv Healthc Mater*, 9:2001410. https://doi.org/10.1002/adhm.202001410
31. Zhao H, Zhang Y, Liu Y, *et al.*, 2021, *In Situ* Forming Cellulose Nanofibril-Reinforced Hyaluronic Acid Hydrogel for Cartilage Regeneration. *Biomacromolecules*, 22:5097–107. https://doi.org/10.1021/acs.biomac.1c01063
32. Sun W, Starly B, Daly AC, *et al.*, 2020, The Bioprinting Roadmap. *Biofabrication*, 12:022002. https://doi.org/10.1088/1758-5090/ab5158
33. Arab W, Kahin K, Khan Z, *et al.*, 2019, Exploring Nanofibrous Self-assembling Peptide Hydrogels using Mouse Myoblast Cells for Three-dimensional Bioprinting and Tissue Engineering Applications. *Int J Bioprinting*, 5:74–82. https://doi.org/10.18063/ijb.v5i2.198
34. Lin C, Wang Y, Huang Z, *et al.*, 2021, Advances in Filament Structure of 3D Bioprinted Biodegradable Bone Repair Scaffolds. *Int J Bioprinting*, 7:43–64. https://doi.org/10.18063/ijb.v7i4.426
35. Zhang X, Liu Y, Zuo Q, *et al.*, 2021, 3D Bioprinting of Biomimetic Bilayered Scaffold Consisting of Decellularized Extracellular Matrix and Silk Fibroin for Osteochondral Repair. *Int J Bioprinting*, 7:85–98.
36. Zheng C, Attarilar S, Li K, *et al.*, 2021, 3D-printed HA15-loaded Beta-Tricalcium Phosphate/Poly (Lactic-co-glycolic acid) Bone Tissue Scaffold Promotes Bone Regeneration in Rabbit Radial Defects. *Int J Bioprinting*, 7:100–11. https://doi.org/10.18063/ijb.v7i1.317
37. Guo Z, Mi S, Sun W, 2019, A Facile Strategy for Preparing Tough, Self-Healing Double-Network Hyaluronic Acid Hydrogels Inspired by Mussel Cuticles. *Macromol Mater Eng*, 304(4):1800715–22. https://doi.org/10.1002/mame.201800715
38. Li Y, Yu P, Wen J, *et al.*, 2022, Nanozyme-based Stretchable Hydrogel of Low Hysteresis with Antibacterial and Antioxidant Dual Functions for Closely Fitting and Wound Healing in Movable Parts. *Adv Funct Mater*, 32:2110720–33. https://doi.org/10.1002/adfm.202110720
39. Zhang J, Wu J, Yu J, *et al.*, 2017, Application of Ionic Liquids for Dissolving Cellulose and Fabricating Cellulose-based Materials: State of the Art and Future Trends. *Mater Chem Front*, 1:1273–90. https://doi.org/10.1039/c6qm00348f
40. Mouser VH, Abbadessa A, Levato R, *et al.*, 2017, Development of a Thermosensitive HAMA-containing

Bio-ink for the Fabrication of Composite Cartilage Repair Constructs. *Biofabrication*, 9:015026. https://doi.org/10.1088/1758-5090/aa6265

41. Siqueira G, Kokkinis D, Libanori R, *et al.*, 2017, Cellulose Nanocrystal Inks for 3D Printing of Textured Cellular Architectures. *Adv Funct Mater*, 27:6926–37. https://doi.org/10.1002/adfm.201604619
42. Hoo SP, Sarvi F, Li WH, *et al.*, 2013, Thermoresponsive Cellulosic Hydrogels with Cell-Releasing Behavior. *ACS Appl Mater Inter*, 5:5592–600. https://doi.org/10.1021/am4009133
43. Zhang Y, Gao C, Li X, *et al.*, 2014, Thermosensitive Methyl Cellulose-based Injectable Hydrogels for Post-operation Anti-adhesion. *Carbohydr Polym*, 101:171–8. https://doi.org/10.1016/j.carbpol.2013.09.001
44. Omidinia-Anarkoli A, Boesveld S, Tuvshindorj U, *et al.*, 2017, An Injectable Hybrid Hydrogel with Oriented Short Fibers Induces Unidirectional Growth of Functional Nerve Cells. *Small*, 13:70191. https://doi.org/10.1002/smll.201770191
45. Kim J, Bae WG, Kim YJ, *et al.*, 2017, Directional Matrix Nanotopography with Varied Sizes for Engineering Wound Healing. *Adv Healthc Mater*, 6:1700297. https://doi.org/10.1002/adhm.201700297
46. Zhou F, Yuan L, Mei Y, *et al.*, 2011, Effects of contact guidance and gravity on L929 cell orientation. *Chinese Sci Bull*, 56:977–81. https://doi.org/10.1007/s11434-010-4173-5

Publisher's note